

# NUMERICAL MODELING OF FLUID DYNAMICS AND HEAT TRANSFER OF GLASS FLOW IN A SHORT CHANNEL

G. E. Ovando Chacon<sup>1\*</sup>, S. L. Ovando Chacon<sup>2</sup> and J. C. Prince Avelino<sup>1</sup>

<sup>1</sup>Instituto Tecnológico de Veracruz, Depto. Metal-Mecánica y Mecatrónica,  
Phone: (+) 52 229 9341500, ext. 136, Calzada Miguel Ángel de Quevedo 2779,  
Col. Formando Hogar, C. P. 91860, Veracruz, Veracruz, México.  
E-mail: ovachag@hotmail.com; jcpa@itv.edu.mx

<sup>2</sup>Instituto Tecnológico de Tuxtla Gutiérrez, Depto. Química y Bioquímica, Phone: (+) 52 961 6150380,  
Carretera Panamericana Km 1080, C. P. 29000, Tuxtla Gutiérrez, Chiapas, México.  
E-mail: ovansandy@hotmail.com

(Submitted: December 5, 2009 ; Revised: April 15, 2010 ; Accepted: August 19, 2010)

**Abstract** - A numerical investigation of laminar flow in a two-dimensional, Cartesian flow that exits from a short channel with a backward-facing step is carried out in this work for the Reynolds number range of  $0.00054 \leq Re \leq 54$ . We studied the steady state fluid dynamics, phase change and heat transfer of the flow. We analyzed the flow behavior occurring for different outflow velocities and three different configuration of the step. The incompressible working fluid was glass. The temperature, streamline, phase change and pressure fields are obtained and analyzed as a function of position. In order to obtain a better understanding of the step angle influence on the fluid dynamics, we obtained the heat transfer flux rates and the axial velocity profiles.

**Keywords:** Numerical simulations; Fluid Dynamics; Heat transfer; Glass; Finite element.

## INTRODUCTION

An important issue in fluid dynamics is the study of fluid flow and heat transfer in channels with phase change, this being the topic of a range of studies because it is present in many technical applications and natural processes. Giessler and Schlegelm (2008) compared a two-dimensional axisymmetric simulation of a glass melt flowing through a pipe with a one-dimensional model. The fluid was supposed to be heated by internal electromagnetic heating and cooled at the wall by convection. It was considered to be a laminar and steady flow of a viscous electrically-conducting fluid in a pipe with circular cross-section driven by a pressure difference between the inlet and the outlet of the pipe. The highly viscous fluid with constant density was supposed to have strongly temperature-dependent

viscosity and electrical conductivity. The steady state flow was governed by the Navier-Stokes equation, the incompressibility condition and the energy equation. The dependence of the mean velocity on the applied pressure difference and the dependence of the mean outlet temperature on the applied pressure difference were analyzed for heating without cooling and cooling without heating. Mirbagheri et al. (2003) simulated the flow of an incompressible molten metal in a mould cavity. They developed a numerical code and proposed a new algorithm with free and solid boundary condition to investigate the heat transfer and the effect of the coating permeability during the mould filling using finite differences. This problem was modeled with the momentum equations, the continuity equation and the heat transfer equation for the liquid or solid zone; the heat transfer equation was used for the

---

\*To whom correspondence should be addressed

mushy region, while the free surface function and the backpressure function were utilized for low melting point metals. Velocity profile, temperature field and filling sequence were obtained from the simulations. To this end, the governing equations were discretized with the finite difference method and a semi-explicit solution of this approximation was obtained to compute the first guess for new time-level velocities using the initial conditions or previous time-level values for all advective, pressure and viscous accelerations. To satisfy the continuity, pressure was iteratively adjusted in each cell and the velocity changes induced by each pressure change are added to the velocity computed previously. In most cases, an over-relaxation factor is used to accelerate the convergence of the iteration. Shmueli et al. (2008) investigated the process of melting of a phase change material in a vertical tube. The numerical simulations were done with fluent and the flow patterns and a detailed distribution of heat transfer on the inner wall of the tube were obtained. The results of the simulation and the analysis of digital pictures, obtained in previous studies, reveal that the effect of convection in the liquid phase provokes non-radial heat fluxes from the wall to the melting zone. The conservation equations for air were solved in the domain bounded by the perimeter of the inner walls, phase change melting from below, and the upper boundary of the tube from above. Boundary conditions for the momentum equation were no-slip at all solid surfaces and slip at the upper boundary of the tube, while for the energy equation constant and uniform temperature on the outside wall of the tube, zero heat flux at the bottom, and ambient air temperature at the upper boundary of the tube were considered. Alexiades et al. (2003) studied the effect of grid and scheme on the numerical solution of a tin melting flow. Simulations were carried out in a square cavity filled with tin (pure metal) initially at freezing temperature (solid tin). The top and bottom boundaries were considered to be adiabatic, while the right boundary was maintained at constant temperature. At the beginning of the simulation, the left boundary was suddenly brought to a hot temperature higher than the melting temperature. Thermal gradients generated density gradients, which provoked convection in the liquid tin. The shape of the solid-liquid interface, the flow pattern in the liquid and the heat transfer process were analyzed. Giannopapa (2006) developed a computational model to simulate the blow-blow forming process of glass containers that characterized the glass flow and the heat transfer. He was able to track the geometry of the deforming

interface of glass applying structured and unstructured fixed meshes. The Navier-Stokes equations were used to describe the motion of the hot glass, while the energy equation was used to describe the heat transfer between the glass and the mould. The governing equations were discretized by the finite element method. In this work, the propagation of glass during the forming process and the temperature profiles were analyzed. Salinas (2006) studied numerically the solidification of aluminum alloy in a square cavity considering the flow of an incompressible Newtonian fluid with isotropic thermal properties where the phase change and the heat transfer by conduction and convection were considered. The mathematical model was based on a set of partial differential equations given by momentum, continuity and heat transfer equations. The discretization of the governing equations was done by the finite volume method combined with a SIMPLER scheme to join pressure and velocities. Transient results of the non-isothermal solidification were obtained and the streamlines and isotherms analyzed, the results showing a complex flow with secondary vorticity. The goal of the present work is to extend the one-dimensional study reported by Jimenez (2002), providing insight into the velocity, the phase change and the temperature fields, as well as to analyze the heat fluxes and axial velocity profiles. The flow is assumed to be two-dimensional because the major changes occur only in the axial and transversal directions. The present research is of particular relevance for the glass industry because we have greatly extended current knowledge on how vortices and heat transfer interact with the geometry of the step channel. Furthermore, this fluid thermal interaction of glass flow underpins much of the behavior of the material properties.

## PROBLEM FORMULATION

We present numerical simulations of the outflowing fluid from a two dimensional axially symmetric short channel with an inclined backward-facing step, as shown in Figure 1.  $\phi$  is the step inclination angle and the fluid enters at the superior boundary of the channel and exits at the inferior boundary of the domain at the outflow velocity denoted by  $U_{out}$ . This velocity is also imposed at the left inferior lateral boundary of the domain to simulate the casting velocity when the fluid is solidified or the jet velocity when the fluid experiments no phase change. No-slip boundary conditions were imposed at all solid walls.

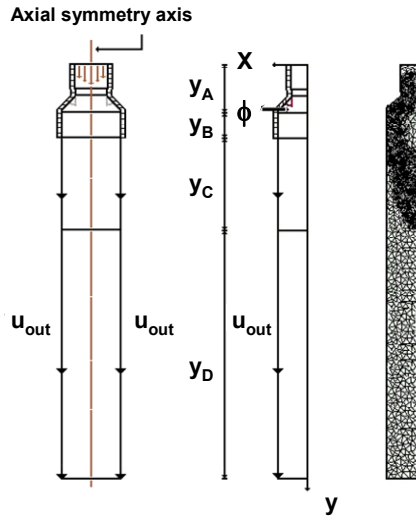


**Figure 1:** Geometry of the channel with inclined backward-facing step and computational adaptive mesh.

The range of outflow velocity explored in this investigation was  $8.65 \times 10^{-5} \text{ m/s} \leq U_{\text{out}} \leq 8.65 \times 10^0 \text{ m/s}$ , which for glass as the working fluid corresponds to the Reynolds number ( $Re = U_{\text{out}} L / \nu$ ) range of  $0.00054 \leq Re \leq 54$ , where  $L$  is the distance from the entrance of the channel to the lower boundary of the domain. The walls of the short channel from the superior part of the channel to the step are assumed to be adiabatic. After the step, convection heat transfer coefficients are imposed along the domain boundary in order to take into account the heat exchange by convection of the glass with the surroundings, which are kept at  $T_0 = 300 \text{ K}$ . At the entrance of the channel, the glass temperature is  $T_m = 1373 \text{ K}$  and the viscous stress vanishes along this boundary. The flow region  $\Omega$  chosen for the numerical simulations is a two-dimensional channel, where the flow, heat transfer and phase change are analyzed. The conservation equations that describe this problem for a steady state incompressible fluid in this region are the momentum, continuity and energy equations:

$$-\nu \Delta \bar{u} + \bar{u} \cdot \nabla \bar{u} + \frac{1}{\rho} \nabla p = \bar{f} \quad \text{in } \Omega, \quad (1)$$

$$\nabla \cdot \bar{u} = 0 \quad \text{in } \Omega, \quad (2)$$

$$\nabla \cdot (-k \nabla T) + \rho C_p \bar{u} \cdot \nabla T = Q \quad \text{in } \Omega, \quad (3)$$

where  $\bar{u} = (u_1, u_2)$  is the velocity vector,  $u_1$  and  $u_2$  being the transversal and axial velocity components respectively;  $\nu$  is the kinematic viscosity,  $p$  is the

pressure,  $k$  is the thermal conductivity,  $C_p$  is the specific heat,  $Q$  is the heating power per unit volume (heat source term) and  $T$  is the temperature.

Because we are interested in the flow behaviour at the phase change interface, the only body force taken into account in this model is given by a Darcian approximation that is a damping force, which ensures zero velocity of the solid phase and is given by the following body force:

$$\bar{f} = \frac{(1 - c_a)^2}{c_a^3 + \varepsilon} c_b (\mathbf{u} - \mathbf{u}_{\text{out}} \hat{j}), \quad (4)$$

where  $c_a$  is the fraction of liquid phase, given by:

$$c_a = \begin{cases} 1 & | (T > T_m + \Delta T) \\ \frac{(T - T_m + \Delta T)}{2\Delta T} & | (T_m - \Delta T) \leq (T_m + \Delta T), \\ 0 & | (T < T_m - \Delta T) \end{cases} \quad (5)$$

$c_b$  is the permeability constant and  $\varepsilon$  is a small number to prevent division by zero in calculations. This term vanishes in the liquid phase region ( $c_a = 1$ ).  $T_m = 1223 \text{ K}$  is the melting temperature and  $\Delta T = 20 \text{ K}$  is the temperature interval where the liquid-solid mixture coexists.

Physically, in the mushy region when the fluid temperature decreases the glass solidifies; as a consequence, the specific heat capacity in the energy equation should be:

$$C_p = C_p + \delta \Delta H, \quad (6)$$

in order to incorporate the effect of the significant amount of latent heat released in the phase change region. On the other hand, most of the released heat occurs near the melting temperature, like a peak of heat due to phase change. Thus, in order to capture this physical phenomenon, we introduce the exponential parameter  $\delta$ , which allows for a pulse type latent heat in the mushy region.  $\delta$  is defined below:

$$\delta = \frac{e^{-(T - T_m)^2 / (\Delta T)^2}}{\Delta T \sqrt{\pi}} \quad (7)$$

while the enthalpy change is given by:

$$\Delta H = T \Delta C_p. \quad (8)$$

The velocity boundary conditions of the channel are:

$$\begin{aligned}
 u_1 &= 0, \quad \frac{\partial u_2}{\partial x} = 0, \quad \text{for } x = 0 \\
 u_1 &= 0, \quad u_2 = 0, \quad \text{for } y_A, y_B \\
 u_1 &= 0, \quad u_2 = u_{\text{out}}, \quad \text{for } y_C, y_D, y_E \\
 u_1 &= 0, \quad u_2 = u_{\text{out}}, \quad \text{for } y = L.
 \end{aligned} \tag{9}$$

The temperature boundary conditions are given by:

$$\begin{aligned}
 \frac{\partial T}{\partial x} &= 0, \quad \text{for } y_A, \\
 h_B &= 35 \text{ W/m}^2 \cdot \text{K}, \quad \text{for } y_B, \\
 h_C &= 105 \text{ W/m}^2 \cdot \text{K}, \quad \text{for } y_C, \\
 h_D &= 60 \text{ W/m}^2 \cdot \text{K}, \quad \text{for } y_D, \\
 h_E &= 40 \text{ W/m}^2 \cdot \text{K}, \quad \text{for } y_E
 \end{aligned} \tag{10}$$

The thermophysical properties of glass used in the simulation are independent of temperature, see Table 1. The data for the glass flow simulated in this work, including the melting temperature and the temperature interval where the liquid-solid mixture coexists, are those for an actual glass and were published by a glass bottle manufacturer (Silices de Veracruz S.A. de C.V) located at Veracruz, Mexico.

**Table 1: Physical properties of glass.**

Property	Glass
Density	2380 kg/m <sup>3</sup>
Specific heat	1235.08 J/kg·K
Thermal conductivity	2.1 W/m·K
Dynamic viscosity	600 Pa·s
Latent heat	205 kJ/kg

## NUMERICAL METHOD

The numerical simulations were carried out using the finite element method. For this purpose, we introduced the space discretization step  $h$ , the finite element triangulation  $\tau_h$  of the polygonal domain  $\Omega$ , the space of polynomials  $P_1$  in two variables of degree less than or equal to one, and the space of continuous functions  $c^0(\bar{\Omega})$  defined in  $\bar{\Omega}$ . The functional spaces are approximated by the following finite dimensional spaces:

$$L_{\text{oh}} = \left\{ q_h \in L_h \mid \int_{\Omega} q_h d\bar{X} = 0 \right\} \text{ with}$$

$$L_h = \left\{ q_h \mid q_h \in c^0(\bar{\Omega}), q_h|_{\tau} \in P_1, \forall \tau \in \tau_h \right\},$$

$$V_{\text{oh}} = \left\{ \bar{v}_h \in V_h \mid \int_{\Omega} \bar{v}_h = 0 \text{ on } \Gamma_1 \right\} \text{ with}$$

$$V_h = \left\{ \bar{v}_h \mid \bar{v}_h \in c^0(\bar{\Omega})^2, \bar{v}_h|_{\tau} \in P_1 \times P_1, \forall \tau \in \tau_{h/2} \right\},$$

and

$$W_{\text{oh}} = \left\{ \theta_h \in W_h \mid \theta_h = 0 \text{ on } \Gamma_3 \right\} \text{ with}$$

$$W_h = \left\{ \theta_h \mid \theta_h \in c(\bar{\Omega}), \theta_h|_{\tau} \in P_1, \forall \tau \in \tau_{h/2} \right\},$$

Using the above finite dimensional spaces leads to the following approximation for Equations (1-3) in their variational forms; for more details, see Chorin (1973), Glowinski and Pironneau (1992), Turek (1999), Marechuk (1990), Glowinski (2003), Glowinski and Le Tallec (1989), Dean and Glowinski (1997), and Dean et al. (1998). For  $t > 0$ , find  $\bar{u}_h(t) \in V_h$  with  $\bar{u}_h(t) = \bar{g}_{1t}(t)$  on  $\Gamma_1$ ,  $p_h(t) \in L_h$  and  $L_h(t) \in W_h$  with  $T_h(t) = g_{3h}(t)$  on  $\Gamma_3$ , such that

$$\int_{\Omega} [(\bar{u}_h \cdot \nabla) \bar{u}_h \cdot \bar{v}] d\bar{X} + \int_{\Omega} \nabla \bar{u}_h : \nabla \bar{v} d\bar{X} -$$

$$\int_{\Omega} p_h \nabla \cdot \bar{v} d\bar{X} = \int_{\Omega} \bar{f} \cdot \bar{v} d\bar{X} \quad \forall \bar{v} \in V_{\text{oh}},$$

$$\int_{\Omega} q \nabla \cdot \bar{u}_h d\bar{X} = 0, \quad \forall q \in L_{\text{oh}},$$

$$\int_{\Omega} [\rho C_p (\bar{u}_h \cdot \nabla) T_h \cdot \theta] d\bar{X} + k \int_{\Omega} \nabla T_h : \nabla \theta d\bar{X} =$$

$$\int_{\Omega} Q \cdot \theta d\bar{X} \quad \forall \theta \in W_{\text{oh}},$$

$$\bar{u}_h(\bar{X}, 0) = \bar{u}_{\text{oh}}(\bar{X}), \quad T_h(\bar{X}, 0) = T_{\text{oh}}(\bar{X})$$

On the other hand,  $\Gamma_1$  and  $\Gamma_3$  are the Dirichlet boundary conditions for velocity and temperature, respectively;  $\bar{g}_{1h}$  and  $g_{3h}$  are the finite element approximations of the velocity and temperature boundary function  $\bar{g}_1$  and  $g_3$ , respectively. Similarly,  $\bar{u}_{\text{oh}}$  and  $T_{\text{oh}}$  are finite element approximations of the initial condition functions  $\bar{u}_0$  and  $T_0$ , respectively.

The simulations were performed with an adaptive mesh for all cases in order to guarantee the mesh independence of the solution. The adaptive mesh

permits fast and accurate calculations because it concentrates the majority of the elements where the phase transition occurs. Figure 2 shows the mesh convergence analysis for three different meshes with resolutions of 17745, 15235 and 10670 net elements. The steady state simulations were obtained with the thinnest mesh using a direct solver with a relative accuracy  $|u^{i+1}-u^i|/|u^{i+1}|$  of  $1.0 \times 10^{-6}$ . The validation of this work was done by the comparison between the present two-dimensional axisymmetric simulation of glass flowing through and leaving from a short channel and the one-dimensional model studied by Jiménez (2002). He analyzed the overheating problem of glass in a short inclined pipe using the thermal resistance approach and considered the convection and conduction heat transfer mechanism. The heat flux rate for  $\phi=50^\circ$  and  $u_{out}=8.65 \times 10^{-2}$  m/s is of the same order of magnitude ( $10^4$  W/m<sup>2</sup>) in both studies.

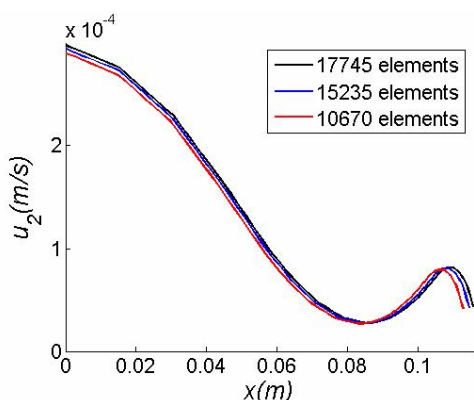


**Figure 2:** Convergence analysis of the axial velocity profile for the outflowing fluid from the short channel for  $\phi=90^\circ$  and  $u_{out}=8.65 \times 10^{-5}$  m/s with three different mesh sizes.

## RESULTS

### CASE $\phi=90^\circ$

Figure 3 shows the temperature, streamline, phase change and pressure fields of the flow that exists from a short channel with a  $90^\circ$  inclined backward-facing step. The flow enters at the superior open boundary and exits at the inferior open boundary of the short channel. Three different outflow velocities  $U_{out}$  are imposed at the left inferior lateral and the inferior boundaries of the domain to simulate the casting velocity or the jet outlet velocity of the fluid according to the phase change. At low outflow velocity  $u_{out}=8.65 \times 10^{-5}$  m/s ( $Re=0.00054$ ), see top left panel of the figure, a uniform pattern of the flow is observed inside the

whole domain. The glass temperature is high at the entrance of the channel and decreases abruptly after the step, with strong gradients of temperature that intensify the heat transfer. Furthermore, the glass temperature decreases significantly after the middle part of the domain. The flow also experiments a phase change, with a liquid phase at the entrance of the channel; however, after the step the fluid becomes solid. The temperature and phase changes are due to the high heat fluxes just after the step of the channel. The pressure field indicates high pressure in the inlet flow region and constant low pressure from the step to the outlet of the domain. Increasing the outflow velocity to  $u_{out}=8.65 \times 10^{-2}$  m/s ( $Re=0.54$ ), see top right panel of the figure, a uniform pattern of the flow is also observed inside the whole domain. However, the glass temperature does not change after the step and remains almost constant through the domain, experimenting a slight change near the wall at the inferior part of the domain. As a consequence of this constant temperature, the flow does not experiment a phase change, a liquid phase being observed through the whole domain. The constant temperature and phase can be associated with the velocity of the fluid, which is sufficiently fast to exchange heat with the surroundings in such a way that there is low total heat transfer. The pressure field indicates no change in the pressure of the flow inside the domain, except for a slight change of pressure at the channel entrances. At high outflow velocity  $u_{out}=8.65 \times 10^0$  m/s ( $Re=54$ ), see bottom panel of the figure, a complex non-uniform pattern of the flow is observed inside the whole domain. Vortex formation can be identified as a consequence of the interaction of the high velocity flow with the step of the channel. The pressure field shows high pressure at the flow inlet, and then the pressure decreases right at the zone where the core of the vortex is located. Finally, the flow increases its pressure and leaves the domain with high pressure. The pressure changes through the channel are due to the perturbation provoked by vortex formation. The maximum velocity in the center of the velocity profile at the inlet of the channel is 6.76% of the imposed outflow velocity for  $u_{out}=8.65 \times 10^{-5}$  m/s, 6.65% of the imposed outflow velocity for  $u_{out}=8.65 \times 10^{-2}$  m/s and 4.27% of the imposed outflow velocity for  $u_{out}=8.65 \times 10^0$  m/s. On the other hand, the outlet temperature of the glass is 27% of the inlet temperature for  $u_{out}=8.65 \times 10^{-5}$  m/s, 98% of the inlet temperature for  $u_{out}=8.65 \times 10^{-2}$  m/s and 100% of the inlet temperature for  $u_{out}=8.65 \times 10^0$  m/s. Values of the maximum velocity at the inlet of the channel and outlet temperature of glass can be seen in Table 2.

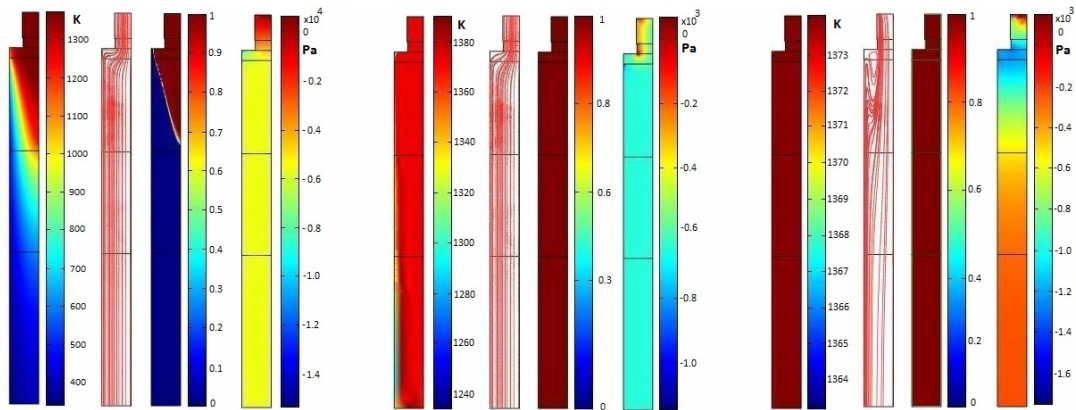


**Figure 3:** Temperature, streamline, phase change and pressure fields for a channel with inclined backward-facing step with  $\phi=90^\circ$ . Left:  $u_{\text{out}}=8.65 \times 10^{-5}$  m/s. Middle:  $u_{\text{out}}=8.65 \times 10^{-2}$  m/s. Right  $u_{\text{out}}=8.65 \times 10^0$  m/s.

**Table 2:** Total heat transfer through the non-adiabatic boundary of the domain, inlet velocity and outlet temperature.

	$u_{\text{cast}}(\text{m/s})$		
	$8.65 \times 10^{-5}$	$8.65 \times 10^{-2}$	$8.65 \times 10^0$
	$\phi=90^\circ$		
W	17514.0	13135.2	53.1
m/s	$5.75 \times 10^{-4}$	$5.75 \times 10^{-1}$	$3.79 \times 10^1$
K	375	1355	1373
	$\phi=50^\circ$		
W	17126.9	120135.5	83.7
m/s	$5.75 \times 10^{-4}$	$5.75 \times 10^{-1}$	$3.82 \times 10^1$
K	372	1347	1373
	$\phi=10^\circ$		
W	27020.3	27138.0	268.5
m/s	$1.33 \times 10^{-4}$	$5.75 \times 10^{-1}$	$3.68 \times 10^1$
K	725	1290	1373

### CASE $\phi=50^\circ$

Figure 4 shows the temperature, streamline, phase change and pressure fields of the flow that exists from a short channel with a  $50^\circ$  inclined backward-facing step with three different outflow velocities of the fluid which are imposed to simulate the casting velocity or the jet outlet velocity of the fluid, depending on the phase change. In these cases, the step of the channel is smoothed to investigate the influence of the step geometry on the fluid behaviour. At low outflow velocity  $u_{\text{out}}=8.65 \times 10^{-5}$  m/s ( $Re=0.00054$ ), see top left panel of the figure, the mushy region where the liquid and solid phase coexist can be clearly observed and the latent heat of fusion is released during the solidification process. However, the pattern of the flow inside the whole domain is uniform. The glass temperature is high at the entrance of the channel and low after the middle

part of the domain, with a strong temperature gradient near the step region. The fluid flow is characterized by three different zones: liquid, mushy and solid zones, the cooling process that takes place in the mushy zone being of great importance from the point of view of material properties. The temperature and phase changes are due to the high heat fluxes just after the step of the channel. The pressure field indicates no change in the pressure of the flow inside the domain. Increasing the outflow velocity to  $u_{\text{out}}=8.65 \times 10^{-2}$  m/s ( $Re=0.54$ ), see top right panel of the figure, a uniform pattern of flow is also observed inside the whole domain. However, the glass temperature and phase do not change after the step and remain almost constant through the domain, experimenting a slight change in the inferior part of the domain where the fluid decreases its temperature and starts to solidify. At high outflow velocity  $u_{\text{out}}=8.65 \times 10^0$  m/s ( $Re=54$ ), see bottom

panel of the figure, vortex formation is also observed due to the interaction of the high velocity flow with the step of the channel, which generates instabilities of the boundary layer located at the step wall. The pressure field shows slight changes in the step zone, the glass temperature is constant and the fluid remains in the liquid phase. The ratio between the maximum velocity in the center of the velocity profile at the inlet of the channel and the imposed outflow velocity of the glass and the ratio between the inlet temperature and the outlet temperature of the glass are practically the same as in the previous case ( $\phi=90^\circ$ ). Values of the maximum velocity at the inlet of the channel and the outlet temperature of glass for this case can also be seen in Table 2.

### CASE $\phi=10^\circ$

In order to describe in detail the effect of the step angle, simulations were done for the flow that exits from a short channel with a  $10^\circ$  inclined backward-facing step. The temperature, streamline, phase change and pressure fields are shown in Figure 5. Three different outflow velocities of the fluid are also explored and imposed at the inferior boundary of the domain to simulate the casting velocity or the jet outlet velocity of the fluid. For a low outflow velocity of  $u_{\text{out}}=8.65 \times 10^{-5}$  m/s ( $Re=0.00054$ ), see top left panel of the figure, the temperature field is more complex than the previous cases with the same outflow velocity. The glass experiments large temperature gradients along the whole domain, which produce an irregular mushy zone that also extends along the domain. This complex interaction between the thermal-fluid dynamic and the geometry of the channel generates liquid-solid interface-breaking. As a result of this irregular behaviour of the phase-change region, the material could modify its properties. The temperature field shows that the hot fluid extends almost until the central part of the domain, while the cold fluid is located in a narrow region near the inferior lower part of the domain. The pressure is high at the inflow region and the streamlines are uniform along the axis of the domain. Increasing the outflow velocity to  $u_{\text{out}}=8.65 \times 10^{-2}$  m/s ( $Re=0.54$ ), see top right panel of the figure, a constant temperature is observed along the whole domain with no phase change and uniform patterns of the fluid. When the outflow velocity is increased to  $u_{\text{out}}=8.65 \times 10^0$  m/s ( $Re=54$ ), see bottom panel of the figure, the vortex distribution and evolution are weaker than those of  $\phi=90^\circ$  and  $\phi=50^\circ$ . The size of the vortices is reduced due to the smooth transition

of the channel, the glass is liquid and its temperature is constant in the whole domain. The fluid experiments reduction of pressure at the step region, with a significant increase of pressure at the outlet of the domain. The pressure pattern at the inlet flow region for  $u_{\text{out}}=8.65 \times 10^2$  m/s and  $\phi=90^\circ$  is different from the pressure pattern of  $\phi=50^\circ$  and  $\phi=10^\circ$  with the same  $u_{\text{out}}$  velocity because, for  $\phi=90^\circ$ , the fluid experiments an abrupt change in the channel step, generating a transversal pressure gradient at the inlet of the channel. The differences of the pressure patterns are due to the perturbation produced by the strong change in the transversal area of the channel with  $\phi=90^\circ$  on the fluid dynamics of glass. Figure 6 shows details of vortex formation due to the sudden change in the flow velocity at the step region for the three different step angles at the largest outflow velocity studied. The flow is characterized by the flow separation from the step corner, which is reduced as the step angle decreases. For  $\phi=90^\circ$  and  $\phi=50^\circ$ , secondary vorticity formed immediately after the primary vortex can be seen, while for  $\phi=10^\circ$ , there is a small vortex without secondary vorticity. The vortical flow is axial, stretched by the inflowing fluid, part of this flow being moved upstream to form the flow recirculation beyond of the step region. This flow reversal is developed just behind the step as a consequence of the separation point in the step corner and the reattachment point on the wall just at the exit of the short channel. For  $\phi=90^\circ$ , one clockwise vortex can be observed near the channel step. The fluid recirculates and mixing takes place in this region; the perturbation is propagated beyond the step, as the streamline suggests. At the core of the vortex, a low pressure zone and stagnation point can be identified and then there is a strong pressure gradient associated with the expansion flow as a result of the abrupt change in the transversal area. For  $\phi=50^\circ$ , one clockwise vortex is produced by the change of the channel transversal section. The inflowing fluid stream splits into a strong central jet and a lateral flow with recirculation and vortex generation. It is seen that the stagnation region decreases and the intensity of the vortices becomes weaker with the reduction of the step angle. The heat transfer phenomena are of the great relevance in flows with detachment and reattachment points because this dynamical behaviour affects the phase change mechanism, which results in a global change of the material properties of the fluid to be solidified. At the zone of the entrance where the geometry expands, the boundary layer detaches due to the strong pressure gradient.



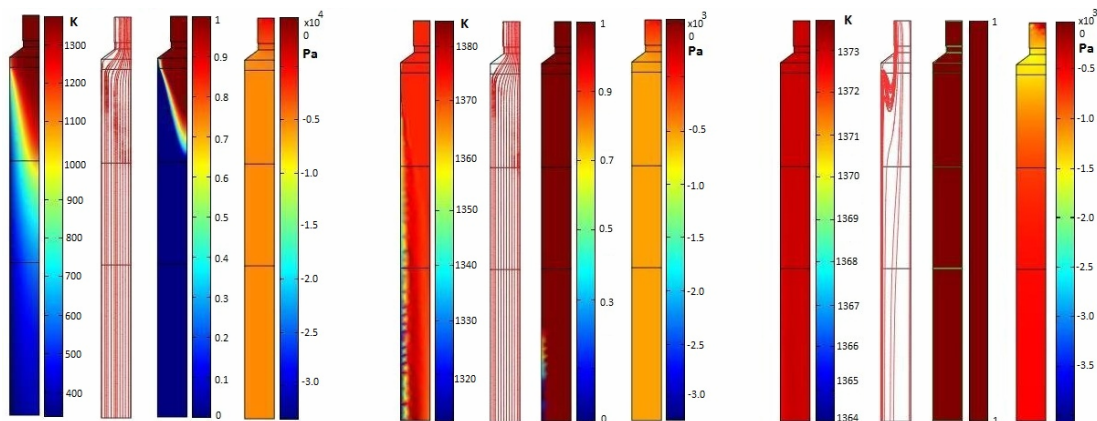


**Figure 4:** Temperature, streamline, phase change and pressure fields for a channel with inclined backward-facing step with  $\phi=50^\circ$ . Left:  $u_{out}=8.65\times 10^{-5}$  m/s. Middle:  $u_{out}=8.65\times 10^{-2}$  m/s. Right  $u_{out}=8.65\times 10^0$  m/s.

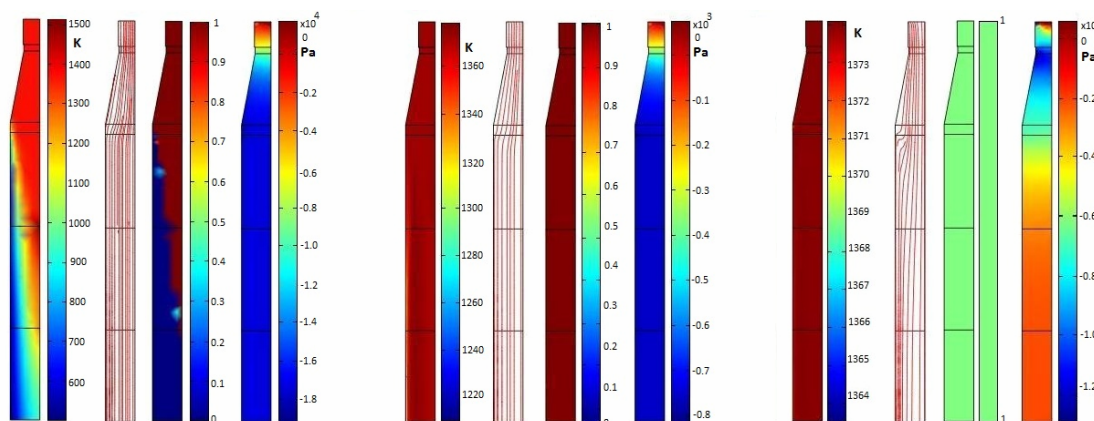


**Figure 5:** Temperature, streamline, phase change and pressure fields for a channel with inclined backward-facing step with  $\phi=10^\circ$ . Left:  $u_{out}=8.65\times 10^{-5}$  m/s. Middle:  $u_{out}=8.65\times 10^{-2}$  m/s. Right  $u_{out}=8.65\times 10^0$  m/s.

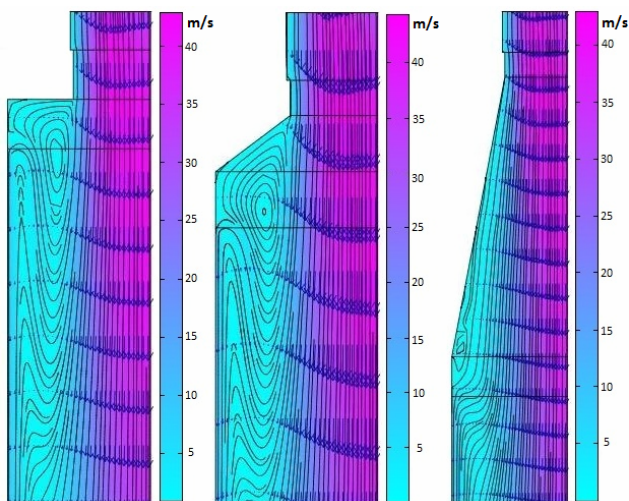


**Figure 6:** Detail of vortex formation for a channel with an inclined backward-facing step and  $u_{out}=8.65\times 10^0$  m/s. Left:  $\phi=90^\circ$ . Middle:  $\phi=50^\circ$ . Right  $\phi=10^\circ$ .



The cooling process of the glass can be seen in Figures 7-9. For the highest outflow velocity,  $u_{out}=8.65 \times 10^0$  m/s, there is a peak of the conductive heat flux at a certain position of the boundary of the domain, these values being  $q_{max}=2541.08$  W/m<sup>2</sup> at  $x=0.2$  m for  $\phi=90^\circ$ ,  $q_{max}=9290.27$  W/m<sup>2</sup> at  $x=0.2$  m for  $\phi=50^\circ$  and  $q_{max}=14598.06$  W/m<sup>2</sup> at  $x=1.6$  m for  $\phi=10^\circ$ . For  $u_{out}=8.65 \times 10^{-2}$  m/s, the heat flux peaks are  $q_{max}=37614.5$  W/m<sup>2</sup> at  $x=0.15$  m for  $\phi=90^\circ$ ,  $q_{max}=96407.7$  W/m<sup>2</sup> at  $x=0.25$  m for  $\phi=50^\circ$  and  $q_{max}=129749.06$  W/m<sup>2</sup> at  $x=1.6$  m for  $\phi=10^\circ$ . For the lowest casting velocity,  $u_{out}=8.65 \times 10^{-5}$  m/s, the maximum released heat occurs near the entrance channel, its values being  $q_{max}=60618.10$  W/m<sup>2</sup> at  $x=0.2$  m for  $\phi=90^\circ$ ,  $q_{max}=68508.4$  W/m<sup>2</sup> at  $x=0.2$  m for  $\phi=50^\circ$  and  $q_{max}=53180.7$  W/m<sup>2</sup> at  $x=0.5$  m for  $\phi=10^\circ$ . The instabilities observed in Figure 8 for  $u_{out}=8.65 \times 10^{-2}$  m/s can be associated with the fluid temperature perturbation in a thin region in the inferior part near the boundary of the domain; in this region, the fluid starts to cool for  $\phi=90^\circ$ . When  $\phi$  decreases to  $50^\circ$ , the instabilities are intensified due to a perturbation not only in the temperature field, but also in the phase change field. In the above two cases, the peak of the perturbation occurs near the exit of the short channel. However, when the step angle is reduced to  $10^\circ$ , the position of the perturbation is moved to the bottom end of the domain. This suggests that the  $\phi$  parameter can be used to control the position of the heat flux instabilities, which can be of major importance for controlling the final properties of the material. In order to get insight into the global cooling process, we compute the total heat transfer through the non-adiabatic boundary of the domain:

$$Q = \int q dA,$$

increasing the outflow velocity of the fluid, the total heat transfer decreases as expected because there is no

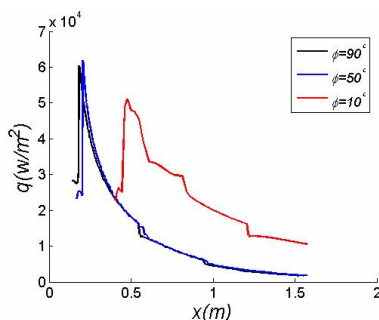


**Figure 7:** Heat fluxes through the non-adiabatic boundary of the domain for  $u_{out}=8.65 \times 10^0$  m/s.

change of phase and the field temperature remains constant. For  $\phi=10^\circ$  the total heat transfer is practically the same for  $u_{out}=8.65 \times 10^{-5}$  m/s and  $u_{out}=8.65 \times 10^{-2}$  m/s. However, there are significant differences of total heat transfer for  $\phi=50^\circ$  and  $\phi=90^\circ$  in the range of  $u_{out}=8.65 \times 10^{-5}$  m/s and  $u_{out}=8.65 \times 10^{-2}$  m/s. Reducing the step angle of the channel increases the total heat transfer. Table 2 shows the values of the total heat transfer for the cases analyzed. In Figures 10 and 11, the axial velocity profiles are shown as a function of the transversal coordinate just after the exit from the short channel for the three different step angles explored with two of the outflow velocities. In all cases, the maximum axial velocity is reached at the center axial line of the channel. Furthermore, this velocity decreases as the transversal coordinate is increased. Figure 12 shows the streamwise velocity profiles as a function of the transversal coordinate for the larger outflow velocity ( $u_{out}=8.65 \times 10^0$  m/s) with the three different configurations of the channel step at different positions of the axial coordinate. In the central part of the domain, the axial velocity of the flow decreases as the fluid moves far away from the step region. For  $\phi=90^\circ$  and  $\phi=50^\circ$ , there is an axial line where the velocity of the flow remains constant (9 m/s); see the point ( $x=0.065$  m) where the profiles cross themselves in the upper and middle panel of the figure. After this point ( $x=0.065$  m), the fluid reduces its axial velocity when  $\phi=90^\circ$  and, near the step, some of these velocities become negative, indicating recirculation of the flow; on the boundary of the domain, the axial velocity is equal to the imposed outflow velocity. This behaviour is maintained for  $\phi=50^\circ$ ; however, in this case the axial velocity on the boundary of the domain is zero due to the non-slip condition imposed at the wall of the channel. For  $\phi=10^\circ$ , the axial velocity profiles cross near  $x=0.065$  m without a constant velocity. In this case, the axial velocity profiles for  $y=0.2$ ,  $y=0.3$ ,  $y=0.4$  are zero and correspond to the velocity of the wall of the channel.

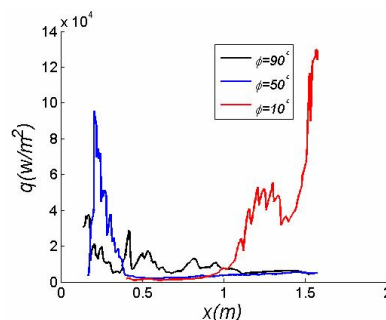


**Figure 8:** Heat fluxes through the non-adiabatic boundary of the domain for  $u_{out}=8.65 \times 10^{-2}$  m/s.

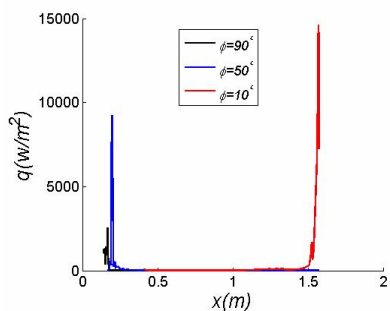


**Figure 9:** Heat fluxes through the non-adiabatic boundary of the domain for  $u_{\text{out}}=8.65 \times 10^0$  m/s.

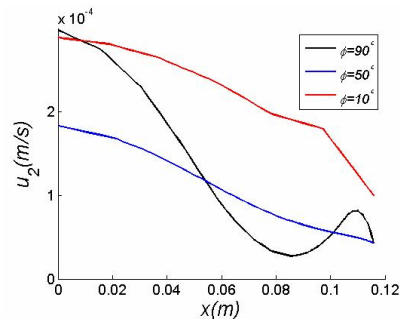


**Figure 10:** Axial velocity profiles as a function of the transversal coordinate just after the exit of the short channel for  $u_{\text{out}}=8.65 \times 10^{-5}$  m/s.

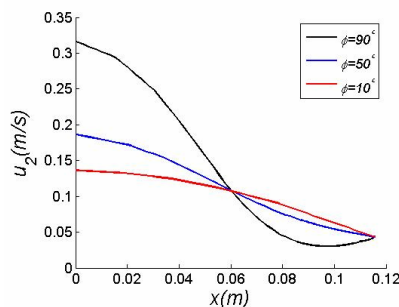


**Figure 11:** Axial velocity profiles as a function of the transversal coordinate just after the exit from the short channel for  $u_{\text{out}}=8.65 \times 10^{-2}$  m/s.

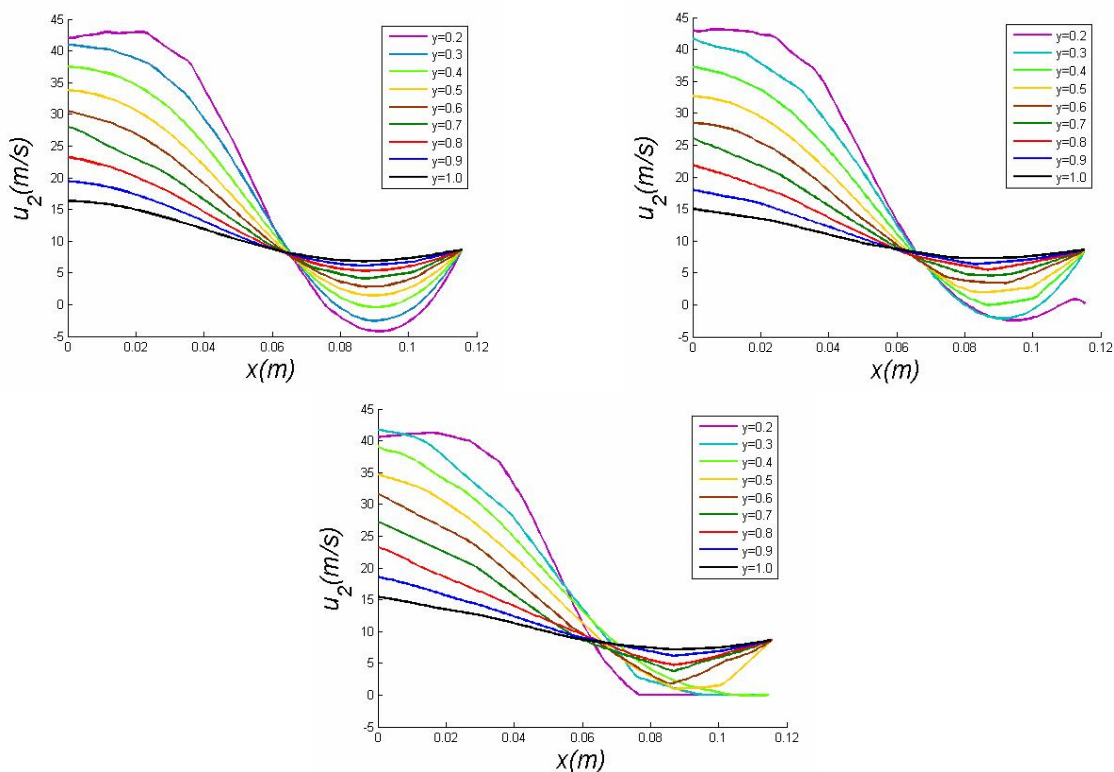


**Figure 12:** Axial velocity profiles as a function of the transversal coordinate for  $u_{\text{out}}=8.65 \times 10^0$  m/s at different position of the axial coordinate. Superior left:  $\phi=90^\circ$ . Superior right:  $\phi=50^\circ$ . Inferior:  $\phi=10^\circ$ .

## CONCLUSIONS

This study was carried out by the numerical solution of the Navier-Stokes equations coupled with the energy equation, using finite element and adaptive meshes. The Darcian approximation was implemented in order to take account of the damping of the velocity when the solidification occurs in a glass flow. We studied the interaction between fluid dynamics, heat transfer and phase change in an outflowing fluid from a short channel with hot temperature at the entrance of the channel. The outflow velocity of the fluid was imposed at the inferior boundary of the domain and on the left inferior lateral boundary of the domain to simulate the casting velocity when the fluid is solidified or the jet velocity when the fluid experiments no phase change. No-slip boundary conditions were imposed at all solid walls. Simulations were performed for three different outflow velocities, characterized by the Reynolds number [ $0.00054 \leq Re \leq 54$ ]. In order to explore the influence of the geometry of the channel step, three different step inclination angles [ $\phi=90^\circ$ ,  $\phi=50^\circ$ ,  $\phi=10^\circ$ ] were analyzed. For low casting or fluid jet velocities, phase change occurs and strong thermal gradients appear near the solidification front to release the latent heat; furthermore, the temperature of the glass decreases gradually along the domain. Upon increasing the step inclination angle, the solidification zone is located near the step region. An important result is given by the fact that breaking of the mushy region occurs for  $\phi=10^\circ$ , characterized by the irregular behaviour of the phase change field. Hence, this fluid dynamics behavior has a significant influence on the final casting quality and solidification sequence. For high casting or fluid jet velocities, the total heat transfer in the fluid is reduced because the fluid does not have time to exchange heat with the surrounding. A low pressure zone appears just at the step region; as a result, the fluid is expanded, reducing the velocity in the process to accommodate for the larger cross-section. The above fluid behaviour produces vortex formation with flow separation from the main stream due to the geometry expansion and a recirculation region appears just in front of the step. The greater the step inclination angle, the greater the intensity of the vortex, which creates secondary vorticity with opposite sign downstream. For  $\phi=90^\circ$  and  $\phi=50^\circ$ , it was found that the heat flux peak occurs near the outlet of the short channel. However, for  $\phi=10^\circ$  the

flux peak occur near the inferior end of the domain as the fluid velocity is increased. Instabilities in the local heat fluxes were observed for  $u_{out}=8.65 \times 10^{-2}$  m/s. Furthermore, decreasing the step angle increases the intensity of the perturbation and the location of these instabilities changes in the domain. The model implemented in this work captures the effect of the fluid velocity associated with the step inclination angle on the phase change process and the conduction heat transfer phenomena for a glass flow in a short channel. So far, this study is limited to the Reynolds number range of [0.00054, 54], but it is useful for understanding heat transfer, phase change and vortex formation in the solidification process of a glass flow. The dynamic behavior beyond this range is the subject of ongoing research. We found that, for a Reynolds number of 0.54 and a step inclination angle of  $\phi=50^\circ$ , the order of magnitude of the heat flux is  $10^4$  W/m<sup>2</sup>; this agrees with the result reported by Jimenez (2002).

## NOMENCLATURE

$c_a$	Liquid phase fraction	
$c_b$	Permeability constant	
$C_p$	Specific heat	J/kg·K
$c^0(\bar{\Omega})$	Continuous function in $\bar{\Omega}$	
$\bar{f}$	Body forces	N/m <sup>3</sup>
$\bar{g}_1$	Dirichlet boundary condition of velocity	m/s
$\bar{g}_3$	Dirichlet boundary condition of temperature	m/s
$\bar{g}_{1h}$	Approximation of velocity Dirichlet boundary	m/s
$\bar{g}_{3h}$	Approximation of temperature Dirichlet boundary	K
$h$	Spatial step	m
$k$	thermal conductivity	W/m·K
$L$	Length	m
$L_{oh}$	Space of trial function for pressure	Pa
$L_h$	Space of finite element trial function for pressure	Pa
$p$	Pressure	Pa
$P_1$	Polynomial space of degree one	
$p_h$	Approximation of pressure finite element	Pa
$q_h$	Trial function of pressure	Pa

Q	Heating power per unit volume	W/m <sup>3</sup>	$\Gamma_3$	Dirichlet boundary of temperature	K
Re	Reynolds number				
T	Temperature	K			
T <sub>m</sub>	Casting temperature	K			
T <sub>out</sub>	Outlet temperature	K			
T <sub>in</sub>	Inlet temperature	K			
T <sub>h</sub>	Approximation of temperature finite element	K			
$\bar{u}$	Velocity vector	m/s			
u <sub>1</sub>	Transversal velocity component	m/s			
u <sub>2</sub>	Axial velocity component	m/s			
$\bar{u}_h$	Approximation of velocity finite element	m/s			
$\bar{v}_h$	Trial function of velocity	m/s			
V <sub>oh</sub>	Space of trial function for velocity	m/s			
V <sub>h</sub>	Space of finite element trial function for velocity	m/s			
W <sub>oh</sub>	Space of trial function for temperature	K			
W <sub>h</sub>	Space of finite element trial function for temperature	K			
$\bar{X}$	Spatial coordinate vector	m			
x	Transversal coordinate	m			
y	Axial coordinate	m			
y <sub>Γ</sub>	Boundary $\Gamma$ on the domain				

### Greek Symbols

$\nabla$	Nabla operator	
$\Delta$	Laplacian operator	
$\rho$	Density	kg/m <sup>3</sup>
$\nu$	Kinematic viscosity	m <sup>2</sup> /s
$\Omega$	Bidimensional region	
$\delta$	Latent heat distribution function	1/k
$\varepsilon$	Small number	
$\Delta T$	Phase change temperature range	K
$\Delta H$	Enthalpy change	J/kg
$\tau$	Finite element triangulation	
$\tau_h$	Finite element triangulation of size h	
$\tau_{h/2}$	Finite element triangulation of size h/2	
$\bar{\Omega}$	Polygonal domain	
$\theta_h$	Trial function of temperature	K
$\Gamma_1$	Dirichlet boundary of velocity	m/s

### ACKNOWLEDGEMENTS

This research was supported by PROMEP grant 103.5/08/2682.

### REFERENCES

- Alexiades, V., Hannoun, N. and Mai, T. Z., Tin melting: effect of grid size and scheme on the numerical solution. Fifth Mississippi State Conference on Differential Equations and Computational Simulations, Electronic Journal of Differential Equations, Conference 10, pp. 55-69 (2003).
- Chorin, A., Numerical study of slightly viscous flow. J. Fluid Mech. 57, pp. 785-796 (1973).
- Dean, E. J. and Glowinski, R., A wave equation approach to the numerical solution of the Navier-Stokes equations for incompressible viscous flow. C. R. Acad. Sci. Paris, 325, Serie I, pp. 789-797 (1997).
- Dean, E. J., Glowinski, R. and Pan, T. W., A wave equation approach to the numerical simulation of incompressible viscous fluid flow modeled by the Navier-Stokes equations. Mathematical and numerical aspects of wave propagation. Edited by J. A. de Santo, SIAM, Philadelphia (1998).
- Giannopapa, C. G., Development of a computer simulation model for blowing glass container. 2006 ASME Conference Proceeding PVP, Vancouver, Canada, pp. 165-172 (2006).
- Giessler, C., Schlegelm, R. and Thess, A., Numerical investigation of the flow of a glass melt through a long circular pipe. International Journal of Heat and Fluid Flow 29, pp. 1462-1468 (2008).
- Glowinski, R., Numerical methods for fluids. Part 3. Handbook of Numerical Analysis, vol. IX, P. G. Garlet and J. L. Lions eds., North-Holland, Amsterdam (2003).
- Glowinski, R., Pironneau, O., Finite element methods for the Navier-Stokes equations, Annual rev. Fluid Mech. 24, pp. 167-204 (1992).
- Glowinski, R. and Le Tallec, P., Augmented Lagrangian and operator-splitting methods in nonlinear mechanics. SIAM, Philadelphia (1989).
- Jiménez, R. A., Análisis del sobrecalentamiento de los vertedores en una máquina de secciones individuales en la fabricación de envases de

- vidrio. M.Sc. Thesis, Veracruz Institute of Technology, Mexico (2002).
- Marechuk, G. I., Splitting and alternate direction methods. Handbook of Numerical Analysis 1, P. G. Garlet and J. L. Lions eds., North-Holland, Amsterdam, pp. 197-462 (1990).
- Mirbagheri, S. M. H., Esmaeileian, H., Serajzadeh, S., Varahram, N. and Davami, P., Simulation of melt flow in coated mould cavity in the casting process. Journal of Materials Processing Technology 142, pp. 493-507 (2003).
- Salinas, C. H., Alloy aluminum solidification in square section. Rev. Fac. Ing. Univ. Tarapacá 14, pp. 16-25 (2006).
- Shmueli, H., Ziskind, G. and Letan, R., Investigation of melting in a vertical circular tube: local heat fluxes. Proceedings of 2008 ASME Summer Heat Transfer Conference, Jacksonville, USA, pp. 1-5 (2008).
- Turek, S., Efficient solvers for incompressible flow problems: An algorithmic and computational approach. Springer-Verlag, Berlin (1999).